ChemComm

ROYAL SOCIETY OF CHEMISTRY

COMMUNICATION

View Article Online
View Journal | View Issue

Check for updates

Cite this: *Chem. Commun.*, 2023, 59, 6008

Received 10th March 2023,
Accepted 17th April 2023

DOI: 10.1039/d3cc01205k

rsc.li/chemcomm

Ultrahigh magnetic resonance contrast switching with water gated polymer–silica nanoparticles†

Daohe Yuan,[a] Connor M. Ellis,[a] Ferenc E. Mózes[b] and Jason J. Davis *[a]

Very high T_1 magnetic resonance imaging (MRI) switches can be obtained with pH-responsive polymer-coated paramagnetic mesoporous silica nanoparticles (MSNs), as the local environment traverses the pK_a of the polymer coat ($\Delta r_1 \sim 50$ mM^{-1} s^{-1} at 1.5 T and $\Delta r_1 \sim 22$ mM^{-1} s^{-1} at 3 T). We assign these characteristics to a strong peripheral hydration capping at the mesopores, impacting channel-confined water mobility such that outer sphere contributions to contrast are greatly enhanced.

Magnetic resonance imaging (MRI) is a powerful non-invasive diagnostic technique with micron spatial resolution and deep tissue penetration that empowers clinicians to resolve and monitor a wide variety of potentially fatal internal pathological conditions.[1,2] Frequent low contrast-to-noise problems can be alleviated through the use of contrast agents (CAs), most notably chelated paramagnetic ions, such as gadolinium(Gd^{3+}).[3] The contrast generating efficiency for a Gd^{3+}-based CA can be defined by its longitudinal relaxivity, denoted r_1 ($r_1 = \Delta(1/T_1)/[\mathrm{CA}]$; where T_1 is the longitudinal relaxation time and [CA] is the concentration of the CA), with a high r_1 correlating to a lower required Gd^{3+} dose, which is, of course, clinically desirable. To improve the natively low molecular r_1 values a broad range of paramagnetically doped nanomaterials, with reduced tumbling rates (τ_R), have been reported.[4] Nanoparticulate CAs additionally present a route to controlled blood circulation times, additional imaging modality incorporation, and tumour accumulation.[5] In prior work, we, and other researchers, have shown that Gd-chelate modified mesoporous silica nanoparticles (Gd-MSNs) offer a synthetically tuneable, and biocompatible, platform with high associated image contrast.[6–12] It has been prior noted that restricted water mobility (elongated diffusional correlation times, τ_D) within the nanoconfinement of a porous reservoir significantly boosts r_1, in large part by increasing the role played by outer sphere effects.[13,14]

Stimuli-responsive "smart" nanoparticulate CAs, where contrast can be switched by an endogenous or exogeneous stimulus, such as light, enzyme activity, redox environment, or local pH,[15] can provide specific information on the local physiological environment, facilitating the ability to distinguish between healthy tissues and lesions, for example.[16,17] In reference to proton relaxation theory,[18,19] tuneable contrast generation can be achieved by the modulation of the diffusive mobility of either inner-sphere (those bound to the metal ions at $\sim$3.1 Å) or outer-sphere (with water-to-Gd distances $\geq$ 4.0 Å) water molecules.[20] For example, a number of switchable nanoparticulate CAs have been designed where the inner-sphere (IS) water exchange rate (τ_M) can be modulated by the local environment.[21–24] Prior reported smart CAs possess, however, only moderate relaxometric switches (*i.e.* $\Delta r_1 < 15$ mM^{-1} s^{-1} and often much less).[25,26] It is also known that relaxivity unhelpfully decreases for typical Gd-based CAs at the higher imaging field strengths that are becoming increasingly common.[20,27] There is, therefore, substantial room to design a high field effective CA that exhibits a significant environmentally triggered switch. To date, no stimuli-responsive CA characteristics have been reported that operate through a modulation of OS contributions.

Herein, we report a versatile surface-initiated reversible addition-fragmentation chain-transfer (SI-RAFT) polymerisation approach to modify Gd-chelate doped MSNs with a stimuli-responsive, externally grafted, polymer shell (Fig. 1a). Poly(methacrylic acid) (pMAA) has been widely reported within pH-responsive drug delivery applications,[28–30] possessing an associated pK_a of 5.2, clinically relevant, for example, to mapping deviations in pH associated with chronic inflammation.[31,32] It is also known that in its charged state pMAA has a particularly strong association with water.[33] It was envisaged that such a capping would impact the mobility of particle internalised water, and hence optimise OS relaxivities (r_1^{OS}).

Initially, paramagnetic Gd-MSNs (with gadolinium (III) 1,4,7,10-tetraazacyclododecane-1,4,7,10-tetraacetic acid, Gd-DOTA, modified pore channels) were synthesised according to

---

[a] *Department of Chemistry, University of Oxford, South Parks Road, Oxford OX1 3QZ, UK. E-mail: jason.davis@chem.ox.ac.uk; Tel: +44 (0)1865 275 914*

[b] *Oxford Center for Clinical Magnetic Resonance Research, Radcliffe Department of Medicine, University of Oxford, Level 0, John Radcliffe Hospital, Oxford, OX3 9DU, UK*

† Electronic supplementary information (ESI) available. See DOI: **https://doi.org/10.1039/d3cc01205k**

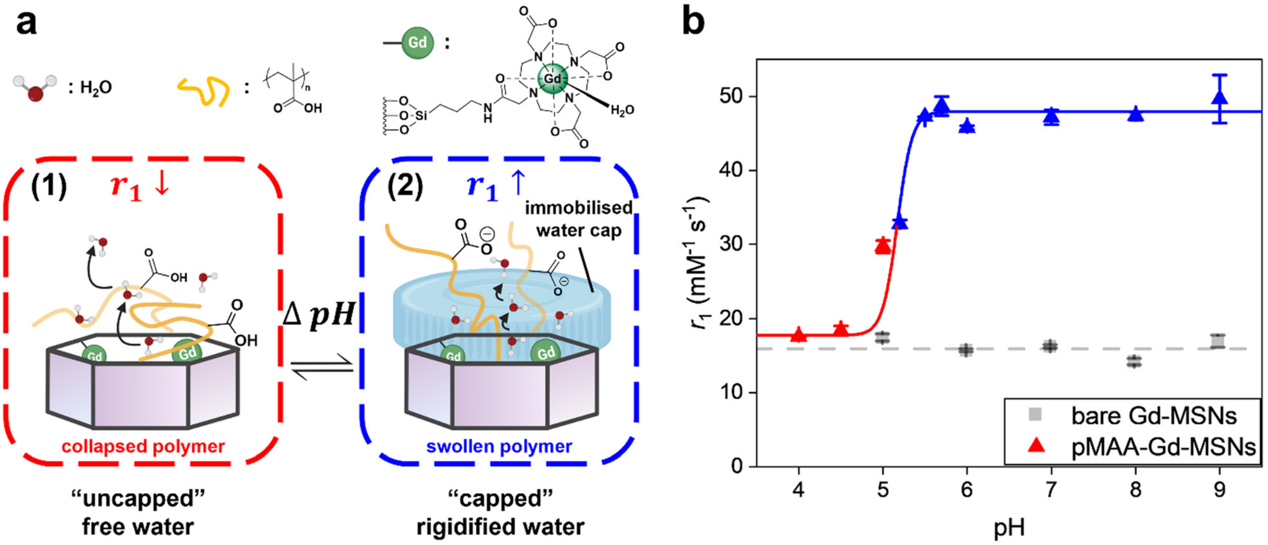

Fig. 1 (a) An illustration highlighting the pH-responsive T_1 switch for pMAA-Gd-MSNs. For an uncharged/collapsed conformation (1), the peripheral pMAA shell possesses limited hydration, and moderate r_1 values. As the polymer shell charges and swells, its hydration increases dramatically, and a ''water cap'' is formed (2). (b) A plot showing the longitudinal relaxivity values (at 1.41 T) for the bare Gd-MSNs and pMAA-Gd-MSNs. The latter exhibits a $\Delta r_1\% > 182\%$, with the r_1 trend fitted using a Boltzmann equation to give an associated estimated p*K*a = 5.2 (R^2 = 0.99) as expected.

prior reports.[34,35] The particles exhibited high colloidal uniformity with an associated size of 49.5 ± 4.2 nm (resolved by transmission electron microscopy, TEM, ESI 1a†) and a corresponding pore diameter of 3.2 ± 0.2 nm (Barrett–Joyner–Halenda pore size analysis, ESI 2†). A time delayed co-condensation method (with 0.15 mol% of an aminated silane added), biases the localisation of amino anchor groups at either the internal or external pore channel, as prior reported.[36] Chemical modification with an activated DOTA-NHS ester and subsequent metalation leads to the generation of the desired paramagnetic MSNs. The outer surface of Gd-MSNs was exclusively modified with a 2-(dodecylthiocarbonothioylthio)-2-methylpropionic acid modified silane (DDMAT-silane) chain transfer agent (CTA), (∼2.9 nm in size, too large to enter the mesopores, ESI 3†). Particle modification was confirmed by ultraviolet-visible spectroscopy (UV-Vis, ESI 4†), thermogravimetric analysis (TGA, ESI 5†) and attenuated total reflectance infrared spectroscopy (ATR-IR, ESI 6†), with a calculated CTA grafting density of *ca.* 4.5 groups nm^{-2} (ESI 7†). This density facilitates the formation of a dense, thickness tuneable (based on RAFT conditions, ESI 8†), polymer brush coating from a wide variety of potential polymerizable monomers.[37–39] The generated polymer coated Gd-MSNs show an observed (and expected) increase in particle diameter after the SI-RAFT polymerisation (TEM, ESI 1b, c, and DLS ESI 8†). The living-character of the polymerisation process was confirmed by proton nuclear magnetic resonance spectroscopy (^{1}H NMR, ESI 9†), where monomer consumption was shown to follow pseudo-first-order kinetics (ESI 9 insets†).[40,41] The generated pMAA-Gd-MSNs possess high colloidal stability, across a broad pH range (in 10 mM Britton-Robinson buffer solution, pH 4.0–9.0), with extremely low polydispersity variation over 30 days (ESI 10,† polydispersity indices < 0.08). An expected pH-responsive switch in hydrodynamic diameter as the pK_a of pMAA[42] is traversed (ESI 8a†). The particles exhibit no toxic effects during a 48 h exposure to HeLa cells or HEK-293T cells (ESI 11†).

Relaxivities of pMAA-Gd-MSNs were first assessed by NMR (1.4 T), where dramatic enhancements in r_1 were observed as the pK_a of pMAA is traversed (Fig. 1b, Δr_1 = 30.3 ± 3.2 $\mathrm{mM}^{-1}\ \mathrm{s}^{-1}$ across 1.0 pH-unit, from pH 4.0 to pH 7.0). This ''switch-on'' response is not observed in the absence of a pMAA polymer coating; native Gd-MSNs exhibit constant relaxivities across the full pH range. In analogous poly(dimethylaminoethyl methacrylate) (pDMAEMA) brush coated particles, where a much weaker H-bond association with bulk water is expected,[43,44] (ESI 12†) the determined relaxivities overlap with those of bare Gd-MSNs and are non-responsive (ESI 13†). For the pMAA particles, associated image contrast enhancements were confirmed through spatially-resolved T_1-mapping experiments on clinical imaging scanners (1.5 T and 3 T; Fig. 2a), with associated T_1 and R_1 values shown in ESI 14.† These switches in r_1 are the highest reported at both magnetic field strengths (Fig. 2b and c, Δr_1 = 50.5 $\mathrm{mM}^{-1}\ \mathrm{s}^{-1}$ at 1.5 T and at Δr_1 = 21.8 $\mathrm{mM}^{-1}\ \mathrm{s}^{-1}$ at 3 T).[25,26] It is also notable that the relaxivities, at both fields, exceed the theoretical maxima for solely IS contributions (optimised r_1^{IS} ∼ 40 $\mathrm{mM}^{-1}\ \mathrm{s}^{-1}$ at 1.5 T and ∼ 20 $\mathrm{mM}^{-1}\ \mathrm{s}^{-1}$ at 3 T),[20,27] suggesting the presence of a composite IS/OS contribution. In fact,[6,45] IS contributions are expected to be much lower than that here (*ca.* 16 $\mathrm{mM}^{-1}\ \mathrm{s}^{-1}$ at 1.5 T, seen ESI 16†). OS contributions are, then, both substantial and responsible for the observed Δr_1 switch (more analyses detailed below).

In examining the effect of polymer thickness and Gd-localisation within the particle mesopores, we note that a larger magnitude switch is observed with thicker polymer shells (at 1.4 T, ESI 17a†) but that switching magnitudes are largely

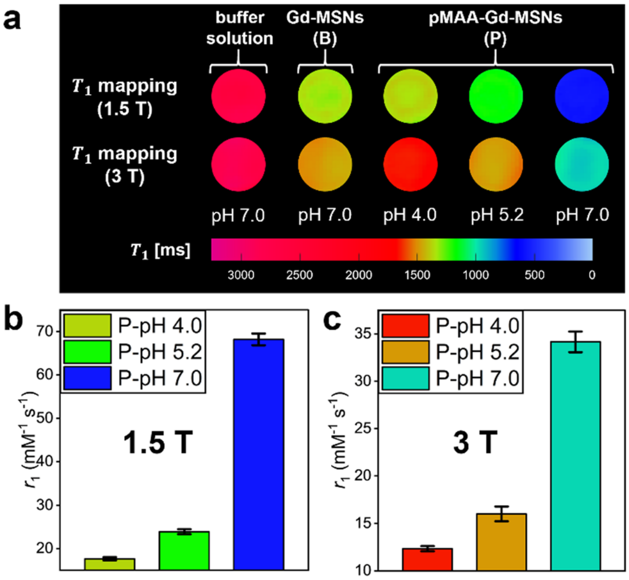

Fig. 2 (a) T_1 maps, recoded at pH 4.0, pH 5.2 and pH 7.0 (1.5 T and 3 T clinical MRI scanners), for the pMAA-Gd-MSNs (denoted as "**P-**"). The T_1 maps for the bare-Gd-MSNs are reported at pH 7.0 (denoted as "**B-**"). The MR derived relaxivities for the associated nanoparticles, across a range of pH, are included at both 1.5 T (b) and 3 T (c).

insensitive to Gd-depth (at 1.4 T, ESI 17b†). This is further confirmatory of a polymer-mediated origin.

To further examine the origin of this large magnitude relaxivity switch we refer to Solomon–Bloembergen–Morgan (SBM) theory (ESI 15†). Contributions from polymer-swelling induced changes in global particle rotation are negligible (ESI 16a†). An analysis of Eu-analogues confirms metal hydration to be the same (ESI 18†) in polymer modified particles at both pH 4.0 and pH 7.0. Additionally, the modulation of the water exchange rate (τ_M) through changes in the conformational state of the polymer cannot fully account for such a high observed switch in the acquired r_1 value. Specifically, the modelled nuclear magnetic relaxation dispersion (NMRD) profile (ESI 16b†) for the IS contribution to r_1 highlights that the role of τ_M is much less significant than the expected influence of τ_D, accounting only for (at best) ~20% of the switch in relaxivity. In recent work the presence of an MSN peripheral immobile water layer has been reported to have a substantial effect on the diffusion coefficient (D) of pore-internal water.[46] It is known that a charged polyacid brush has an unusually strong association with water, dramatically reducing its mobility.[47,48] Within a modified SBM model (ESI 15†), an entirely realistic (30–90 fold) reduction in internal water diffusion, D, can account for the enhancement in relaxivity (Fig. 3). We propose, then, that the triggered polymer charging generates a peripheral particle water "cap" that dramatically increases OS relaxivity by virtue of its impact on particle internalised water.

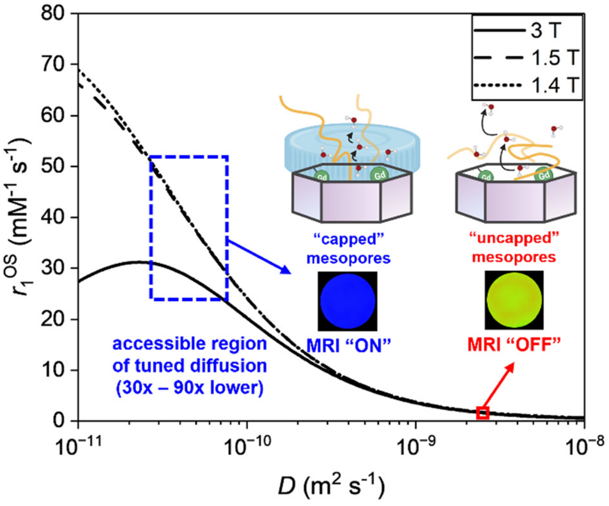

Fig. 3 The effect of the local diffusion coefficient of water on the outer-sphere relaxivity. This analytical treatment employs a modified Freed equation (at 1.4, 1.5 and 3 T), and considers the diffusion of water at r_{GdH} = 4.0 Å from the paramagnetic centres (ref. 49). The diffusion coefficient of confined H_2O with "uncapped" mesopores is taken from ref. 46. The diffusion coefficient of confined H_2O with capped mesopores is deduced from the experimental relaxivity data, where D is observed to be reduced by 30–90x.

To summarise, we present here paramagnetic inorganic-organic hybrid nanoparticles that exhibit a pH-mediated contrast switch that is sharp (across < 1.0 pH-unit), of an unprecedented magnitude, clinically relevant, and mechanistically new.

The authors would like to thank Shaoyu Kang, Department of Chemistry, University of Oxford for Gaussian optimisation and helpful discussions, Dr Robert Jacobs, Surface Analysis Facility, Department of Chemistry, University of Oxford for surface analysis assistance, Shijun Yan, Nuffield Department of Clinical Neurosciences, University of Oxford for cell viability assistance and Trang To, School of Geography and the Environment, University of Oxford for ICP-MS data.

Conflicts of interest

There are no conflicts of interest to declare.

References

1 D. Ni, W. Bu, E. B. Ehlerding, W. Cai and J. Shi, *Chem. Soc. Rev.*, 2017, **46**, 7438–7468.
2 J. Wahsner, E. M. Gale, A. Rodríguez-Rodríguez and P. Caravan, *Chem. Rev.*, 2019, **119**, 957–1057.
3 T. J. Clough, L. Jiang, K.-L. Wong and N. J. Long, *Nat. Commun.*, 2019, **10**, 1420.
4 J. Pellico, C. M. Ellis and J. J. Davis, *Contrast Media Mol. Imaging*, 2019, 1845637.
5 N. Zhao, L. Yan, X. Zhao, X. Chen, A. Li, D. Zheng, X. Zhou, X. Dai and F.-J. Xu, *Chem. Rev.*, 2019, **119**, 1666–1762.
6 F. Carniato, L. Tei, M. Cossi, L. Marchese and M. Botta, *Chem. – Eur. J.*, 2010, **16**, 10727–10734.
7 F. Carniato, L. Tei, A. Arrais, L. Marchese and M. Botta, *Chem. – Eur. J.*, 2013, **19**, 1421–1428.
8 K. M. L. Taylor, J. S. Kim, W. J. Rieter, H. An, W. Lin and W. Lin, *J. Am. Chem. Soc.*, 2008, **130**, 2154–2155.
9 F. Carniato, L. Tei and M. Botta, *Eur. J. Inorg. Chem.*, 2018, 4936–4954.
10 D. Yuan, C. M. Ellis and J. J. Davis, *Materials*, 2020, **13**, 3795.
11 F. Tang, L. Li and D. Chen, *Adv. Mater.*, 2012, **24**, 1504–1534.
12 W.-Y. Huang, G.-L. Davies and J. J. Davis, *Chem. Commun.*, 2013, **49**, 60–62.

13 J. S. Ananta, B. Godin, R. Sethi, L. Moriggi, X. Liu, R. E. Serda, R. Krishnamurthy, R. Muthupillai, R. D. Bolskar, L. Helm, M. Ferrari, L. J. Wilson and P. Decuzzi, *Nat. Nanotechnol.*, 2010, **5**, 815–821.
14 P. H. Fries and E. Belorizky, *J. Chem. Phys.*, 2010, **133**, 024504.
15 C. M. Ellis, J. Pellico and J. J. Davis, *Materials*, 2019, **12**, 4096.
16 C. d l H. Alarcón, S. Pennadam and C. Alexander, *Chem. Soc. Rev.*, 2005, **34**, 276–285.
17 Y. Lu, A. A. Aimetti, R. Langer and Z. Gu, *Nat. Rev. Mater.*, 2016, **2**, 16075.
18 I. Solomon, *Phys. Rev.*, 1955, **99**, 559–565.
19 N. Bloembergen and L. O. Morgan, *J. Chem. Phys.*, 1961, **34**, 842–850.
20 P. Caravan, C. T. Farrar, L. Frullano and R. Uppal, *Contrast Media Mol. Imaging*, 2009, **4**, 89–100.
21 L. Zhu, Y. Yang, K. Farquhar, J. Wang, C. Tian, J. Ranville and S. G. Boyes, *ACS Appl. Mater. Interfaces*, 2016, **8**, 5040–5050.
22 J. Pellico, C. M. Ellis, J. Miller and J. J. Davis, *Chem. Commun.*, 2019, **55**, 8540–8543.
23 C. Caro, M. L. García-Martín and M. Pernia Leal, *Biomacromolecules*, 2017, **18**, 1617–1623.
24 Y. Li, Y. Qian, T. Liu, G. Zhang and S. Liu, *Biomacromolecules*, 2012, **13**, 3877–3886.
25 G.-L. Davies, I. Kramberger and J. J. Davis, *Chem. Commun.*, 2013, **49**, 9704–9721.
26 S. Fu, Z. Cai and H. Ai, *Adv. Healthcare Mater.*, 2021, **10**, 2001091.
27 L. M. De León-Rodríguez, A. F. Martins, M. C. Pinho, N. M. Rofsky and A. D. Sherry, *J. Magn. Reson. Imaging*, 2015, **42**, 545–565.
28 P. Yang, D. Li, S. Jin, J. Ding, J. Guo, W. Shi and C. Wang, *Biomaterials*, 2014, **35**, 2079–2088.
29 B. Tian, S. Liu, W. Lu, L. Jin, Q. Li, Y. Shi, C. Li, Z. Wang and Y. Du, *Sci. Rep.*, 2016, **6**, 21335.
30 Y. Q. Yang, X. D. Guo, W. J. Lin, L. J. Zhang, C. Y. Zhang and Y. Qian, *Soft Matter*, 2012, **8**, 454–464.
31 S. R. Bonam, F. Wang and S. Muller, *Nat. Rev. Drug Discovery*, 2019, **18**, 923–948.
32 F. Wang and S. Muller, *Front. Immunol.*, 2015, **6**, 252.
33 S.-P. Ju, W.-J. Lee, C.-I. Huang, W.-Z. Cheng and Y.-T. Chung, *J. Chem. Phys.*, 2007, **126**, 224901.
34 W. Stober, A. Fink and E. Bohn, *J. Colloid Interface Sci.*, 1968, **26**, 62–69.
35 J. J. Davis, W. Y. Huang and G. L. Davies, *J. Mater. Chem.*, 2012, **22**, 22848–22850.
36 M. J. Hollamby, D. Borisova, P. Brown, J. Eastoe, I. Grillo and D. Shchukin, *Langmuir*, 2012, **28**, 4425–4433.
37 J. O. Zoppe, N. C. Ataman, P. Mocny, J. Wang, J. Moraes and H.-A. Klok, *Chem. Rev.*, 2017, **117**, 1105–1318.
38 R. Ranjan and W. J. Brittain, *Macromol. Rapid Commun.*, 2008, **29**, 1104–1110.
39 K. Ohno, Y. Ma, Y. Huang, C. Mori, Y. Yahata, Y. Tsujii, T. Maschmeyer, J. Moraes and S. Perrier, *Macromolecules*, 2011, **44**, 8944–8953.
40 A. Goto, K. Sato, Y. Tsujii, T. Fukuda, G. Moad, E. Rizzardo and S. H. Thang, *Macromolecules*, 2001, **34**, 402–408.
41 M. J. Flanders and W. M. Gramlich, *Polym. Chem.*, 2018, **9**, 2328–2335.
42 X. Wang, X. Ye and G. Zhang, *Soft Matter*, 2015, **11**, 5381–5388.
43 S. H. Min, S. K. Kwak and B.-S. Kim, *Soft Matter*, 2015, **11**, 2423–2433.
44 R. Chockalingam and U. Natarajan, *Mol. Phys.*, 2015, **113**, 3370–3382.
45 L. Tei, G. Gugliotta, Z. Baranyai and M. Botta, *Dalton Trans.*, 2009, 9712–9714.
46 M. Weigler, E. Winter, B. Kresse, M. Brodrecht, G. Buntkowsky and M. Vogel, *Phys. Chem. Chem. Phys.*, 2020, **22**, 13989–13998.
47 H. S. Sachar, T. H. Pial, P. R. Desai, S. A. Etha, Y. Wang, P. W. Chung and S. Das, *Matter*, 2020, **2**, 1509–1521.
48 H. S. Sachar, B. S. Chava, T. H. Pial and S. Das, *Macromolecules*, 2021, **54**, 2011–2021.
49 M. Botta, *Eur. J. Inorg. Chem.*, 2000, 399–407.